UDC 624.014.2 **doi:10.31650/2707-3068-2025-29-47-54**

WORKING FEATURES AND RELIABILITY OF METAL SPIRAL-FOLD SILOS

Pichugin S., DSc, Professor
pichugin.sf@gmail.com ORCID 0000-0001-8505-2130,
National University "Yuri Kondratyuk Poltava Polytechnic"
Oksenenko K., PhD, design engineer
shvadchenkokate@gmail.com ORCID 0000-0002-5171-3583
LLC "Architectural Engineering Center"

Annotation. The article comprehensively discusses an innovative metal sheet structure - a spiral fold silo: its features, operation under load, and reliability. The stress-strain state of interfold zone of a spiral-fold silo is considered. The calculations of the stress-strain state of the silo were compared with the analytical calculations by the software package LIRA-SAPR. The work the midsection of the shell segment (zone between folded locks) of the spiral-fold silo was experimentally verified. Considering the results of the studies of the stress-strain state of this metal silos, a methodology for reliability analysis based on the analysis of the strength reserve was developed. The obtained results of calculations confirmed the high reliability of metal spiral-fold silos.

Keywords: spiral-fold silo, stress-strain state, experimental study, reliability analysis.

Introduction. The calculation theories of thin-walled storage capacities, such as the spiral-fold silos that are discussed in this article, were developed based on studies by the steel sheet structures. The main specificity of sheet metal structures is their ability to be used in various conditions: structures can be above ground, below ground, semi-buried, underground, or underwater; sheet metal structures can withstand static and dynamic loads; structures must work reliably under low, medium and high pressure, under vacuum, under the influence of low, medium and high temperatures, neutral or aggressive environments. Considering the above features, the structural variation of steel sheet structures is clear, which can be classified as follows: gas holders, tanks, large diameter pipelines, silos, protective shell structures, and special sheet structures.

Taking into account the structural variety of sheet metal structures, the following types of their stress state are distinguished: momentless stress state, when the equilibrium of the shell is ensured only by stresses evenly distributed over the shell thickness; moment stress state, when the equilibrium of the shell is ensured by bending stresses (relatively rare for thick shells); edge effect - local bending of individual sections of sheet metal structures.

Analysis of recent researches and publications. A number of scientists have studied the calculation methods and experimental studies of metal spiral-fold silos for strength and stability.

In 2008, S. Wirth [1] used the experimental results of small spiral-fold silos to analyze the possibility of using the EN 1993-1-6 standard [2] for bending of shells. He concluded that it is quite difficult to numerically determine the resistance close to the experimental results in accordance with the requirements of EN 1993-1-6.

A significant contribution to the study of spiral-fold silos are made by A. Jäger-Cañás (consulting engineer at Lipp GmbH), Z. Li, and H. Pasternak. Their works [3, 4] are devoted to the study of thin shells with frequently horizontal ribs. This type of shell includes both spiral-fold silos and any other containers with horizontal ribs. For instance, in work [3], experimental studies are described on small cylindrical shells, which were made by welding two semicylindrical shells, and the annular stiffeners were welded to the cylindrical shell by spot welding.

The geometric dimensions of the shell specimens were measured using 3D scanning technology. The obtained data on geometric imperfections were directly integrated into the numerical model through a mapping correlation. The results demonstrated that the bending resistance computed via finite element analysis closely matched the experimental findings. The primary focus of these

studies is the behavior of the inter-stiffener regions of the shell under axial compression and the effect of closely spaced horizontal stiffeners on the overall strength and stability of silo structures.

Identification of previously unresolved parts of the general problem to which the article is devoted. A review of available studies on spiral-fold silos reveals a lack of comprehensive research dedicated to these innovative structural systems. In particular, investigations that holistically examine design features, their influence on the stress–strain state, and reliability assessment have yet to be conducted.

The aim of the research. The aim of this study is to analyze the stress–strain behavior of steel spiral-fold silos and to compare theoretical and analytical calculations in order to gain a deeper understanding of their structural performance and reliability.

Results and discussion. The design of spiral-fold silo shells differs significantly from other types of steel storage containers, such as prefabricated metal silos made of corrugated panels with bolted joints, or welded steel tanks. Their unique structural features [5] affect not only the stress-strain behavior but also the overall performance of the structure. As a result, these silos are highly versatile, cost-effective, and efficiently used for storing various types of bulk materials, liquids, or as digesters in bioenergy facilities [6–9].

A characteristic feature of spiral-fold silos is their thin-walled nature ($^{r}/_{t} = 1000 \div 4500$), where *r* is a radius and *t* is wall thickness, which necessitates detailed strength analysis of the wall.

The analytical model (Fig. 1, a) of the entire silo is represented as a system of short shell segments connected by closed-type horizontal spiral-fold stiffeners (folded locks). These short shell segments are referred to as shell segments.

Due to the presence of spiral-fold horizontal stiffeners, the longitudinal force is transmitted to the silo wall with eccentricity, leading to the development of additional bending moments. These moments, in turn, cause wall deformation in the inter-fold zones.

The analysis of the silo wall should be carried out based on the deformed configuration (Fig. 1,b), as simplified geometrically linear methods fail to reflect the actual structural behavior and do not provide a sufficient safety margin. These simplified methods neglect the additional bending moments induced by the geometrically nonlinear deformation of the silo shell. The presence of radial deflection in the inter-fold zones also leads to a reduction in the load-bearing capacity of the wall, both in terms of stability and strength.

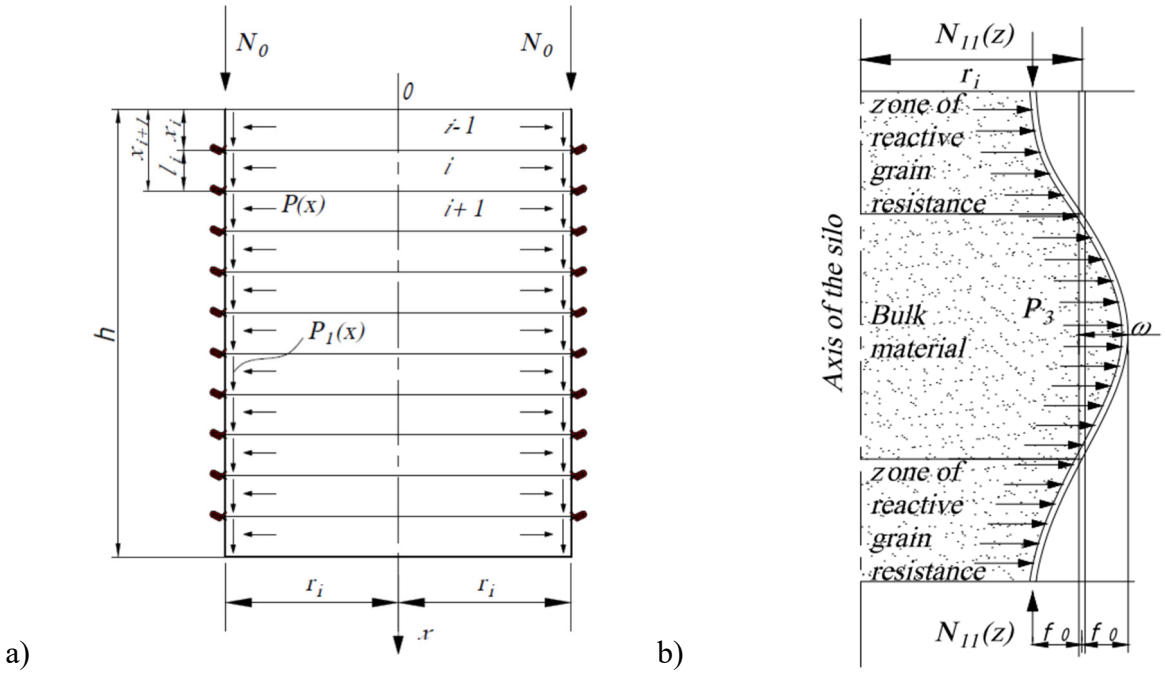

a) b)

Fig. 1. Calculation of the spiral-folded silo: a) calculation scheme; b) deformed calculation scheme of the silo under strength analysis, considering the initial outward deflection of the silo

In the development of the computational model, the governing equations of longitudinal-transverse bending with respect to radial displacements were employed for a symmetrically loaded shell. The following variables were used as primary parameters: $P(x)$, $P_1(x)$ are, respectively, the horizontal and vertical pressure of the bulk material; $N_1(x)$ is the longitudinal force from the vertical pressure of the bulk material $P_1(x)$, the weight of the wall N_{01}, and the load from the roof structure N_0, $\omega(x)$ is deflection (radial displacement) in the shell; $M(x)$ is longitudinal bending moment in the shell; $\sigma^u(x), \sigma^k(x)$ are longitudinal and hoop stresses, respectively.

The horizontal and vertical pressure of the bulk material are determined by the following expressions:

$$P(x) = P_h^n = \frac{\gamma\rho}{f}[1 - exp(-\lambda f x/\rho)], P_1(x) = P_f^n = fP_h^n,$$

where ρ is the hydraulic radius of the cross-section of the silo, *m*, which is determined by the formula $\rho = A/U$; *A, U* are area and perimeter of the silo cross-section; λ is the lateral pressure ratio of particulate solids; γ is bulk unit weight; P_h^n is normative horizontal pressure.

According to DBN V.2.2-8-98 [10] the longitudinal force $N_1(x)$ induced by the vertical bulk material pressure acting on the silo bottom $P_v^n(x)$, as well as by the self-weight of the shell N_{01} and the roof structure N_0 is computed using the following expression:

$$N_1(x) = \rho(\gamma x - P_v^n) + N_{01}(x) + N_0, N_{01}(x) = \gamma_s trz,$$

where γ_s denotes the specific weight of the shell material.

The governing differential equation for the longitudinal-transverse bending equilibrium of the symmetrically loaded cylindrical shell with respect to radial displacements is expressed as follows:

$$\omega^{IV}(x) + 4\beta^4\omega(x) = P(x) + \frac{\nu N_1(x)}{r} - e \cdot \frac{dP_1(x)}{dx}), \quad (1)$$

where $4\beta = \frac{Et}{Dr^2}$, $\beta = \sqrt[4]{\frac{3(1-\nu^2)}{r^2t^2}}$, D is cylindrical stiffness, $D = \frac{Et^3}{12(1-\nu^2)}$, E is modulus of elasticity of the shell material, ν is Poisson's ratio, t is wall thickness, r is radius of the silo.

Since integration is more convenient when performed using expressions in dimensionless form, the equilibrium equations of a symmetrically loaded cylindrical shell (1) are transformed to a dimensionless coordinate system $\xi = \beta x$.

$$\omega^{IV}(\xi) + 4\omega(\xi) = \frac{1}{\beta^4 D}\Phi(x), \quad (2)$$

where $\Phi(x)$ is the load function, defined as, $\Phi(x) = P(x) + \frac{\nu N_1(x)}{r} - e \cdot \frac{dP_1(x)}{dx})$, e is the distance from the line of action of the shear forces to the mid-surface of the shell.

The solution to the differential equation governing the longitudinal-transverse bending of the shell segment (2) is expressed in the following form:

$$\omega(\xi) = C_1V_1(\xi_i) + C_2V_2(\xi_i) + C_3V_3(\xi_i) + C_4V_4(\xi_i) + \frac{1}{4\beta^4 D}\int_0^{\xi} V_4(\xi_i - \xi_{il})\Phi(\xi_{il})d\xi_{il}, \quad (3)$$

where C_1, C_2, C_3, C_4 are the constants of integration; $V_1(\xi_i), V_2(\xi_i), V_3(\xi_i), V_4(\xi_i)$ are fundamental functions of Krylov O.M. [11]

Let us consider the stress–strain state of a shell segment (can) subjected to the reactive forces of elastic spiral-fold stiffeners, under the combined action of the following loads:

- horizontal pressure $P(x)$ and vertical pressure $P_1(x)$ from the bulk material;
- constant longitudinal compressive force N_0, representing the vertical load from superimposed structures;
- variable longitudinal compressive force $N_{01}(x)$ due to the self-weight of the shell wall;
- eccentrically applied shear forces with respect to the mid-surface of the shell.

To simplify the analysis, the following assumptions are introduced:

- stiffeners (folded locks) are arranged horizontally;
- the silo shell consists of individual shell segments bounded by the stiffeners;

– within each shell segments, $P = const$, $N_{01} = const$;
– the stiffeners are elastic and extend in the radial direction, with radial displacement $\omega_0 = \frac{T_r^2}{EA}$ where T_r is the reactive longitudinal force and A is the cross-sectional area of the stiffener (folded lock).

After performing the corresponding transformations, the radial deflection and longitudinal bending moment are determined at characteristic sections of the *i*-th shell segment — specifically, at the shall segment edges and at its midsection:

a) at $\xi = \tilde{\xi} = 0$ ($\xi = \tilde{\xi} = \beta l_1$) – on the edge of the shell segment:

$$\omega(\tilde{\xi}) = \frac{(P+\nu N_1/r-eP_1)r^2}{EA} \cdot \frac{n_2(\tilde{\xi})}{\frac{t}{A}n_2(\tilde{\xi})+\frac{\beta}{2}n_3(\tilde{\xi})}; \quad (4)$$

$$M(\tilde{\xi}) = \frac{(P+\nu N_1/r-eP_1)r^2}{2\beta} \cdot \frac{n_1(\tilde{\xi})}{\frac{t}{A}n_2(\tilde{\xi})+\frac{\beta}{2}n_3(\tilde{\xi})}; \quad (5)$$

b) at $\xi = \bar{\xi} = \beta l_1/2$ – at the midsection of the shell segment:

$$\omega(\bar{\xi}) = \frac{(P+\nu N_1/r-eP_1)r^2}{Et} \cdot \left[1 + \frac{2\beta n_5(\bar{\xi})}{\frac{t}{A}n_2(\bar{\xi})+\frac{\beta}{2}n_3(\bar{\xi})}\right]; \quad (6)$$

$$M(\bar{\xi}) = -\frac{(P+\nu N_1/r-eP_1)r^2}{2\beta} \cdot \frac{n_4(\bar{\xi})}{\frac{t}{A}n_2(\bar{\xi})+\frac{\beta}{2}n_3(\bar{\xi})}, \quad (7)$$

where $n_4(\bar{\xi}) = V_2(\bar{\xi})n_2(\bar{\xi}) - V_1(\bar{\xi})n_1(\bar{\xi}) - V_3(\bar{\xi})n_3(\bar{\xi})$;
$n_5(\bar{\xi}) = n_1(\bar{\xi})V_3(\bar{\xi}) - n_2(\bar{\xi})V_4(\bar{\xi}) - \frac{1}{4}n_3(\bar{\xi})V_1(\bar{\xi})$

After calculating the radial deflection and bending moment at the characteristic sections of the *i*-th shell segment (Equations 4–7), the hoop forces are determined at the shell segment edges and at its midsection:

$$N_s(\tilde{\xi}) = \frac{Et}{r}\omega(\tilde{\xi}) - \nu N_1; \quad (8)$$

$$N_s(\bar{\xi}) = \frac{Et}{r}\omega(\bar{\xi}) - \nu N_1. \quad (9)$$

The fiber longitudinal and hoop stresses $\sigma^u(\tilde{\xi}), \sigma^k(\tilde{\xi})$ are determined at the edge and at the midsection of the shell segment:

a) at $\xi = \tilde{\xi} = 0$ ($\xi = \tilde{\xi} = \beta l_1$) – on the edge of the shell segment:

$$\sigma^u(\tilde{\xi}) = \frac{N_1}{t} \pm \frac{M(\tilde{\xi})}{W}; \quad (10)$$

where $W = \frac{t^2}{6}$;

$$\sigma^k(\tilde{\xi}) = \frac{N_s(\tilde{\xi})}{t}; \quad (11)$$

b) at $\xi = \bar{\xi} = \beta l_1/2$ – at the midsection of the shell segment:

$$\sigma^u(\bar{\xi}) = \frac{N_1}{t} \pm \frac{M(\bar{\xi})}{W}; \quad (12)$$

$$\sigma^k(\tilde{\xi}) = \frac{N_s(\tilde{\xi})}{t}. \quad (13)$$

The intensity of the fiber stresses is assessed using the maximum values of the longitudinal and hoop stresses.

$$\frac{\gamma_m}{R_y\gamma_c}\sqrt{\sigma_u^2(\xi)-\sigma_u(\xi)\sigma_k(\xi)+\sigma_k^2(\xi)} \le 1. \quad (14)$$

The stress-strain state of the midsection of the shell segment (between the folded locks) with a constant wall thickness is considered. The section is elastically connected to the adjacent shell segments and experiences a stress-strain state of longitudinal-transverse bending type.

To compare the theoretical calculations with the results obtained using the finite element method, a model was created in the LIRA-SAPR software package. The model consists of 3 tiers of spiral-fold shell segments, with a tiers height of 36.5 cm, a shell radius of r = 4 *m*, wall thickness of t = 4 *mm*, and the cross-sectional area of the folded lock for a 4 mm thick strip A=7,35 cm^2. The material of the shell is steel C235, with a yield strength $R_y(x) = 235МПа$, elastic modulus $E = 2{,}1 \cdot 10^5 MPa,$ and Poisson's ratio ν (not specified in the original text). For simplification, only the horizontal pressure from the bulk material $P(x) = 2{,}74\frac{H}{cm^2}$ was applied to the structure.

Calculations were performed according to the algorithm described above. Based on formulas (4) and (6), the following deflection values were obtained: at the edge of the shell segment $\omega(\tilde{\xi}) = 0{,}37mm$; at the midsection $\omega(\bar{\xi}) = 0{,}466mm$.

To validate the theoretical results, a finite element model was developed in the LIRA-SAPR software environment using the previously specified shell parameters. A general view of the model is shown in Figure 2. The wall tiers between the ring stiffeners were modeled using shell finite elements of type 44 (“quadrilateral shell element”), oriented in the vertical plane, with a thickness of 4 *mm* and an elastic modulus corresponding to steel grade C235. The spiral-fold stiffener was modeled using type 41 shell elements (“rectangular shell element”) with a cross-sectional area of 7,35 cm^2.

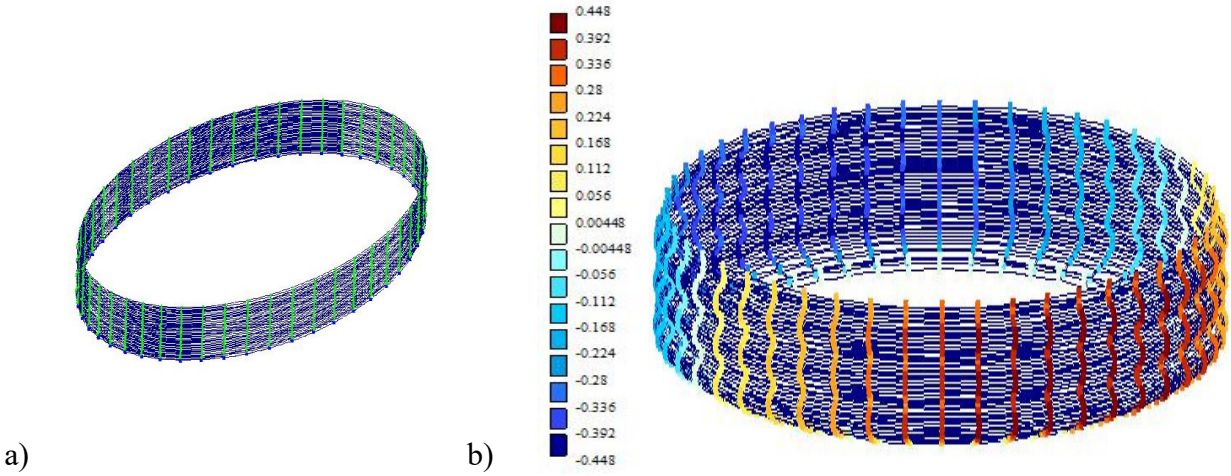

a) b)

Fig. 2. Finite element model in LIRA-SAPR:
a) Finite element model; b) Displacement mosaic of the shell nodes

The deflections obtained from the LIRA-SAPR simulation are as follows: at the edge of the shell segment $\omega = 0{,}353mm$; at the midsection $\omega = 0{,}448mm$. The mosaic of displacements for the shell under horizontal pressure, as calculated in LIRA-SAPR, is shown in Figure 3. The values are represented using a dimension-color scale (in millimeters) displayed on the left side of the figure.

The difference between the analytically calculated deflections using formulas (4) and (6) and those obtained from the LIRA-SAPR model is: at the edge of the shell segment 4,8%; at the midsection 3,8%.

Considering all the structural features of spiral-fold silos and their influence on the stress–strain state, it becomes evident that detailed investigation of the bending behavior in the interfold zone of the shell wall is of critical importance. To reveal the actual bending performance of the wall in a spiral-fold silo, an experimental study was carried out. The objective of the research was to experimentally determine the deformation evolution of the folded lock during loading and to assess

the stress–strain state of the silo wall at different stages of bending. This experimental investigation is described in detail in [12].

The obtained results were compared with a finite element analysis performed using the LIRA-SAPR software suite. For the simulation, the parameters of the experimental specimen were used. The silo wall and the folded stiffening rib were modeled using flat shell finite elements of type 44 ("quadrilateral shell element").The dimensions of the finite elements were 9 *mm* × 10 *mm* (Figure 3).To ensure consistency between the computational model and the experiment, the ends of the model were fixed (clamped).

a)

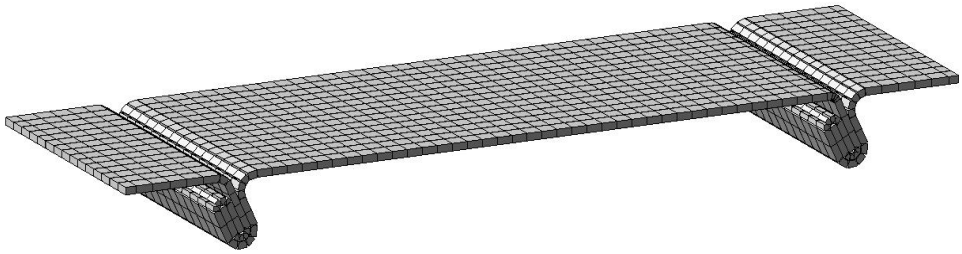

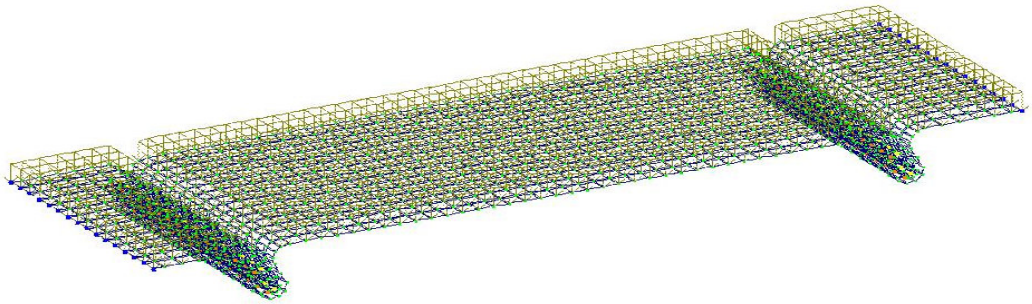

b)

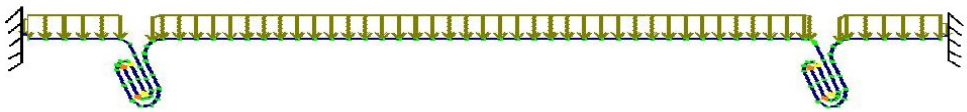

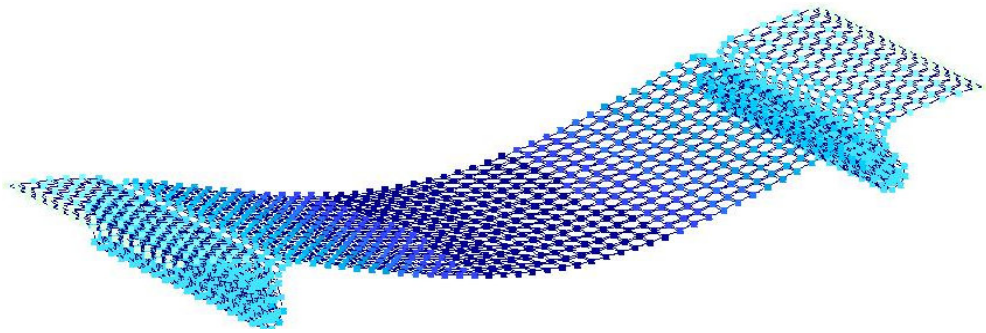

c)

Fig. 3. Modeling of the experimental specimen in LIRA-SAPR:
a) 3D model; b) model loading; c) displacement mosaic.

When the modeled specimen (Figure 3a) was loaded with a uniformly distributed load corresponding to the experimental conditions, deflection–load curves for the interfold zone were constructed (Figure 4). The graph shows that when the load increases to 2.5 kN and above, the experimental specimens exhibit greater deflections than the numerical results. This discrepancy is attributed to the opening of the folded seam, which is not accounted for in the computational model. In summary, the difference in interfold zone deflections between the experimental specimen and the finite element analysis results ranges from 3% to 5%.

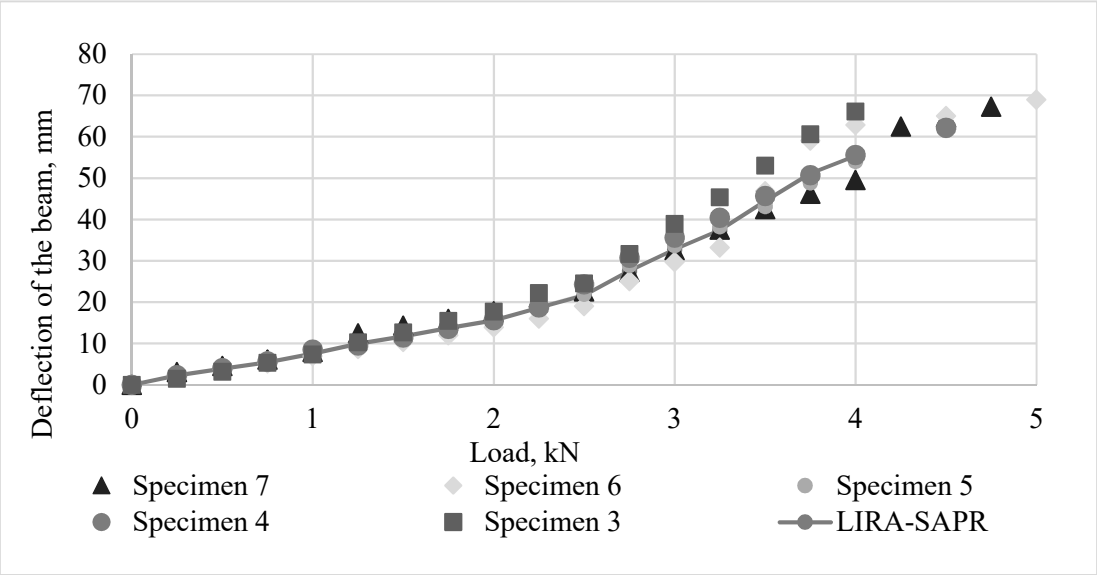

Fig. 4. Graph of the deflection-load relationship of the specimen in the interfold zone.

Based on the conducted and above-described studies, a methodology was developed for assessing the reliability of a spiral-fold metal silo using an analysis of the strength reserve factor $\tilde{Y}$, taking into account its stress–strain state [13]. The obtained numerical results confirmed the high reliability of spiral-fold metal silos.

Conclusions:

1. The article provides a comprehensive review of the innovative metal sheet structure – the spiral-folded silo.

2. The stress–strain state of the interfold zone of the spiral-fold silo is examined. A comparison of the results from the finite element method (FEM) with analytical calculations from the LIRA-SAPR software suite was carried out. The difference between the analytically calculated deflections using formulas (4) and (6) and those obtained from the LIRA-SAPR model is: at the edge of the shell segment 4,8%; at the midsection 3,8%.

3. An experimental verification of the behavior of the interfold zone of the shell and the adjacent folded locks of the spiral-fold silo was performed.

4. Taking into account the results of the stress–strain analysis of the metal spiral-fold silos, a methodology for assessing their reliability based on the strength reserve analysis was developed. The obtained calculation results confirmed the high reliability of metal spiral-fold silos.

References

[1] Wirth S., “Beulsicherheitsnachweise für schalenförmige Bauteile nach EN 1993-1-6: Kritische Analyse der praktischen Anwendbarkeit anhand zweier Fallstudien mit experimentellem Hintergrund“: Thesis: University of Duisburg-Essen, Shaker Verlag. 2008.

[2] ДСТУ-Н Б EN 1993-1-6:2011 Єврокод 3. Проектування сталевих конструкцій. Частина 1 – 6. Міцність та стійкість оболонок. К. : Мінрегіонбуд, 2011. 146 с.

[3] Li Z., Pasternak H., Jaeger-Canas A. Buckling of ring-stiffened cylindrical shell under axial compression: Experiment and numerical simulation. Thin-walled structures. 2021. Vol. 164. P. 107888.

[4] Jäger-Cañás A, Pasternak H. Influence of closely spaced ring-stiffeners on the axial buckling behavior of cylindrical shells. EUROSTEEL 2017. September 13–15, Copenhagen, Denmark. 2017.

[5] Pichugin S., Oksenenko K., Hajiyev M., Sulewska M., January 2021, “Features of structures and calculation of steel spiral-fold silos”., E3S Web of Conferences. vol. 280(4):03006. DOI: 10.1051/e3sconf/202128003006.

[6] Xaver Lipp [Internet resource]. Available: https://xaver-lipp.com/.
[7] S. Pichugin, K. Oksenenko. “Using of spiral-fold silos on the territory of Ukraine”, ArCivE 2021, pp 430 – 437, 2021.
[8] Pichugin S., Oksenenko K. Area of application and operation experience of spiral-fold silos in Ukraine. ArCivE 2023. Xth International scientific conference on architecture and civil engineering. Varna, 2023. Vol. 4. P. 14 – 22.
[9] Pichugin S., Oksenenko K. Spiral-fold Silo is Innovative Storage for Wood Chips. AIP Conference Proceedings. 2023. Vol. 2678. P. 020013. doi.org/10.1063/5.0118821.
[10] ДБН В.2.2-8-98. Підприємства, будівлі та споруди по зберіганню та переробці зерна. К.: Держбуд України. 1998. 41 с.
[11] Birger I.A., Shorr V.F., Shneiderovich R.M. Strength calculation of machine parts. Moscow: Mechanical Engineering. 1966. 590 p.
[12] Пічугін С., Шульгін В., Оксененко К. Експериментальне дослідження напружено-деформованого стану стінки сталевого спірально-фальцевого силосу. Сучасні будівельні конструкції з металу та деревини. 2023. Вип. 27. С. 94-103. doi:10.31650/2707-3068-2023-27-94-103.
[13] Pichugin S., Oksenenko K. The reliability analysis of metal spiral-fold silos. Modern building structures made of metal and wood. 2024. Issue 28. P. 172-182. doi:10.31650/2707-3068-2024-28-172-182

ОСОБЛИВОСТІ РОБОТИ ТА НАДІЙНІСТЬ МЕТАЛЕВИХ СПІРАЛЬНИХ СИЛОСІВ

Пічугін С.Ф., д.т.н., професор,
pichugin.sf@gmail.com ORCID 0000-0001-8505-2130,
Національний університет «Полтавська політехніка імені Юрія Кондратюка»
Оксененко К.О., доктор філософії, інженер-проєктувальник
shvadchenkokate@gmail.com ORCID 0000-0002-5171-3583
ТОВ «Архітектурно-інженерний центр»

Анотація. У статті комплексно розглянуто інноваційну металеву листову конструкцію – спірально-фальцевий силос: його особливості, робота під навантаженням, надійність. Розглянуто напружено-деформований стан проміжної ділянки (між фальцевими ребрами) оболонки з постійною товщиною стінки. Ділянка пружно з’єднана з сусідніми обичайками та зазнає напружено-деформований стан типу поздовжньо-поперечного згину. У результаті аналізу було наведено формули прогину та поздовжнього згинаючого моменту у характерних перерізах і-ї обичайки – по краях та в середині. Проведено порівняння теоретичних розрахунків напружено-деформованого стану з розрахунками методом скінченних елементів у програмного комплексі ЛІРА-САПР. У результаті було отримано, що різниця значень переміщень, розрахованих за допомогою формул (4), (6) та визначених у програмному комплексі ЛІРА-САПР складає: на контурі обичайки – 4,8%; у середині обичайки – 3,8%.

Проведено експериментальну перевірку роботи міжфальцевої зони оболонки та прилеглих фальцевих замків спірально-фальцевого силосу. Для підтвердження результатів експерименту було виконано порівняння експериментальних залежностей із розрахунком методом скінченних елементів у програмному комплексі ЛІРА-САПР. Підсумовуючи отримані дані, можна стверджувати, що різниця між переміщеннями міжфальцевої зони експериментального зразка та розрахунками методом скінченних елементів складає 3 – 5 %.

З врахуванням результатів проведених досліджень напружено-деформованого стану металевих спірально-фальцевих силосів розроблено методику оцінювання надійності на основі аналізу резерву міцності. Одержані результати розрахунків підтвердили високу надійність металевих спірально-фальцевих силосів.

Ключові слова: спірально-фальцевий силос, напружено-деформований стан, експериментальне дослідження, оцінювання надійності.